Coherent Smith-Purcell radiation for minimally invasive bunch length measurement at the subpicosecond time scale

Philipp Heil[ORCID],[*] Kurt Aulenbacher, Christoph Matejcek, Simon Friederich[ORCID],
Max Bruker[ORCID],[†] and Frank Fichtner

Institute for Nuclear Physics, Johannes Gutenberg University Mainz, Germany,
Helmholtz Institute Mainz, Germany
and GSI Helmholtzzentrum für Schwerionenforschung, Darmstadt, Germany

We have designed a tool to measure the bunch length of an electron beam in a minimally invasive way by means of coherent Smith-Purcell radiation (SPR). The technique has been employed successfully at a test apparatus for the Mainz Energy-recovery Superconducting Accelerator *MESA*, demonstrating it is possible to determine the bunch length while losing less than 0.6% of the electron beam. The impact of the space charge on the bunch length can be reduced while tuning the longitudinal bunch preparation system during a live measurement at beam currents up to 1 mA. Doing so, RMS bunch lengths of 70 μm can be achieved in a typical operating mode of the low-energy beam transport system of MESA. In addition to the bunch length measurements, typical properties of the generated SPR are demonstrated.

I. INTRODUCTION

In order to investigate ultrafast physical processes, short pulses of particles have been receiving more and more attention. In accelerator physics, short electron bunches are needed to ensure acceleration of the beam without losing too many particles or, in other words, to match the accelerator acceptance. In preparation for the construction of the Mainz Energy-recovery Superconding Accelerator (*MESA*), we have built a test apparatus comprising the first ten meters of the low-energy beam transport system at 100 keV of *MESA*. As the longitudinal bunch preparation system is installed here, this apparatus is suitable for bunch length measurements, even at high beam currents. In those circumstances, Coulomb interactions between the electrons lead to a blow-up of the whole bunch (space charge).

II. GENERATION OF COHERENT SPR

If a charged particle passes by a metallic grating in close proximity, its evanescent field excites multiple resonant modes in the groove of the grating profile. These modes emit plane waves above the surface of the grating. An

approach to calculating the power of the emitted SPR by solving Maxwell's equations with the periodic boundary conditions of the grating is described in the papers by van den Berg ([1] and [2]). Figure 1 shows a schematic sketch of the electron beam passing a grating at the distance z_0. For semirelativistic particles ($\beta = 0.548$) the wavelength λ of the emitted radiation is in the order of magnitude of the grating period D and is dependent on the observation angle η and the order of diffraction n [3].

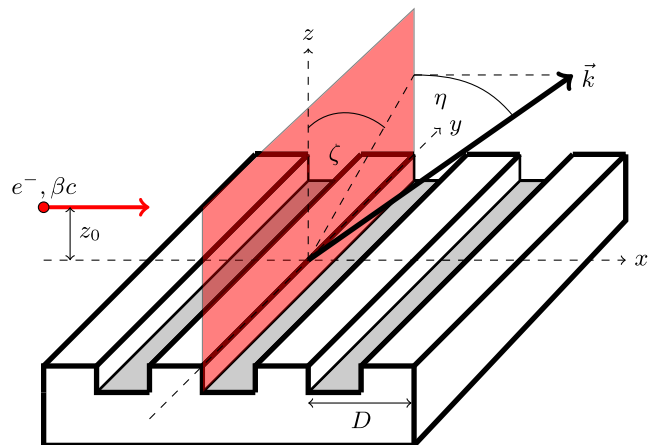$$\lambda = \frac{D}{n}\left(\frac{1}{\beta} - \sin\eta\right) \tag{1}$$

FIG. 1. Arrangement to produce SPR with corresponding coordinates and angles. $\vec{k}$ is the vector where SPR is observed.

[*]phheil@uni-mainz.de
[†]Present address: Thomas Jefferson National Accelerator Facility, Newport News, Virginia 23606, USA.

The wavelength is not dependent on the azimuth angle ζ. The power of the emitted radiation per solid angle can be calculated using van den Berg's approach [4].

$$
\frac{dP}{d\Omega} = \frac{IN_w e |n|^2 \beta^3 \cos^2\eta\cos^2\zeta}{2D\epsilon_0(1-\beta\sin\eta)^3} \cdot |R_n(\eta,\zeta)|^2 \cdot [S_{\text{inc}}(\eta,\zeta)
$$
$$
+ (N_e - 1)S_{\text{coh}}(\eta,\zeta)], \tag{2}
$$

where N_w is the number of grating periods, I is the beam current, e the elementary charge, ϵ_0 the vacuum permittivity, R_n a reflection coefficient dependent on the geometry of the grating, N_e the number of electrons per bunch, and S_{inc}, S_{coh} the coherent and incoherent part of the radiation, respectively. S_{coh} is dependent on the charge distribution $f_z(z)$, $f_y(y)$ and $f_x(x)$ of the electron bunch in space. The distribution in the longitudinal direction $f_x(x)$ can be expressed in terms of time $f_t(t)$ with the known velocity of the particles βc.

$$
S_{\text{coh}} = \left| \int_0^\infty \exp\left[-\frac{z}{2h_{\text{int}}(\eta,\zeta)}\right] f_z(z) dz \right|^2
$$
$$
\times \cdot \left| \int_{-\infty}^\infty e^{-ik_y y} f_y(y) dy \right|^2 \cdot \left| \int_{-\infty}^\infty e^{-i\omega t} f_t(t) dt \right|^2, \tag{3}
$$

where the first term is governed by the ratio of the distance of the beam center from the grating surface and the interaction length h_{int}:

$$
h_{\text{int}}(\eta,\zeta) = \frac{D(1/\beta - \sin\eta)}{4\pi|n|\sqrt{1/\beta^2 - 1 + \cos^2\eta\sin^2\zeta}} \tag{4}
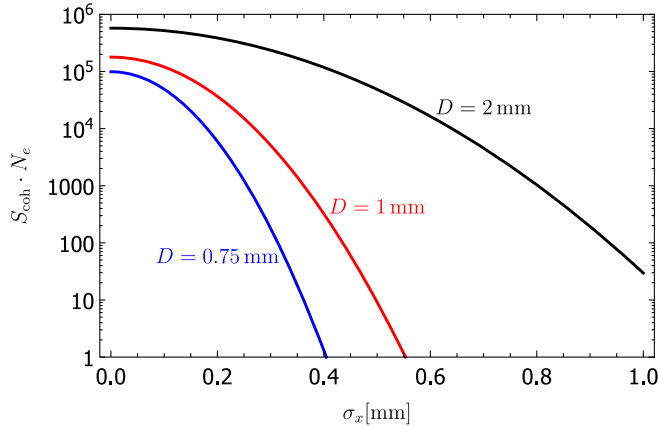$$

FIG. 2.   Coherent enhancement factor $N_e \cdot S_{\text{coh}}$ for different bunch lengths $\sigma_x = \beta c \sigma_t$ and grating periods D in the first radiation order ($n = 1$). Coherent SPR can only be observed if the bunch length σ_x is smaller or comparable to half the grating period D. These curves show the effect of different values of $h_{\text{int}}(D)$, while the charge distribution of the beam is the same in each case.

The second term is approximately equal to one because the transverse size of the beam is much smaller than the width of the grating. The third term is defined by the charge distribution in the longitudinal direction $f_t(t)$, where $\omega = 2\pi c/\lambda$ and c is the speed of light in vacuum. We assume the charge distributions $f_t(t)$ and bunch lengths σ_t to be Gaussian. For $\beta = 0.548$, S_{coh} becomes significant and approaches one for $\sigma_t \beta c \leq D/2$, and a coherent enhancement of the radiation by a factor of N_e occurs. Figure 2 shows $N_e \cdot S_{\text{coh}}$ for a beam current of $I = 1$ mA, corresponding to a particle number of $N_e = 5 \times 10^6$. In this experiment, the incoherent part of the SPR cannot be observed because its intensity is below the background level; only coherent SPR can be observed, the power of which is in the order of pW to nW. Because coherent SPR is emitted only if the bunch length $\sigma_x \lesssim D/2$, placing gratings with different periods D next to the beam yields an upper bound of the bunch length. A comparison of the calculated power with the measured one gives even more precise results.

III. BEAM LINE SETUP AND PARAMETERS

An important part of the new accelerator *MESA* is the low-energy beam transport system *MELBA* (Mesa low-energy beam apparatus) connecting the 100 keV electron source with the injector accelerator. Here, spin manipulation and bunch preparation for the injector take place. Due to the low energy, space charge is a challenging issue. A test setup has been built to check the functionality of devices and compare the beam parameters with the simulation [5–7]. The overall layout of the setup is shown in Fig. 3.

The electron beam is generated by emitting electrons from a GaAs photocathode using laser radiation at a wavelength of 800 nm and accelerating them with a DC voltage of 100 kV [8]. In this experiment, the laser operates in DC mode and thus provides a continuous electron beam. The following beam line contains the longitudinal bunch preparation system, which converts this DC beam into short electron bunches using a system of two circularly deflecting 1.3 GHz chopper cavities and a system of first- and second-harmonic buncher cavities. This system is based on that employed at *MAMI* [9] and adapted to the *MESA* rf frequency. With two buncher cavities, the injector can make use of a larger fraction of an incoming DC beam than would be achievable with a single cavity; this is particularly important for spin-polarized operation where the amount of charge that can be extracted during the cathode lifetime is limited. To characterize the longitudinal bunch profile in a minimally invasive fashion, an SPR diagnostic chamber is installed downstream of the buncher after a drift space of about 1.5 m. This location corresponds to the beginning of the pre-accelerator in the case of *MESA*.

The diagnostic device is designed to generate and observe the coherent part of SPR [10]. In our experiment, the interesting range of bunch charges is between 0.1 and
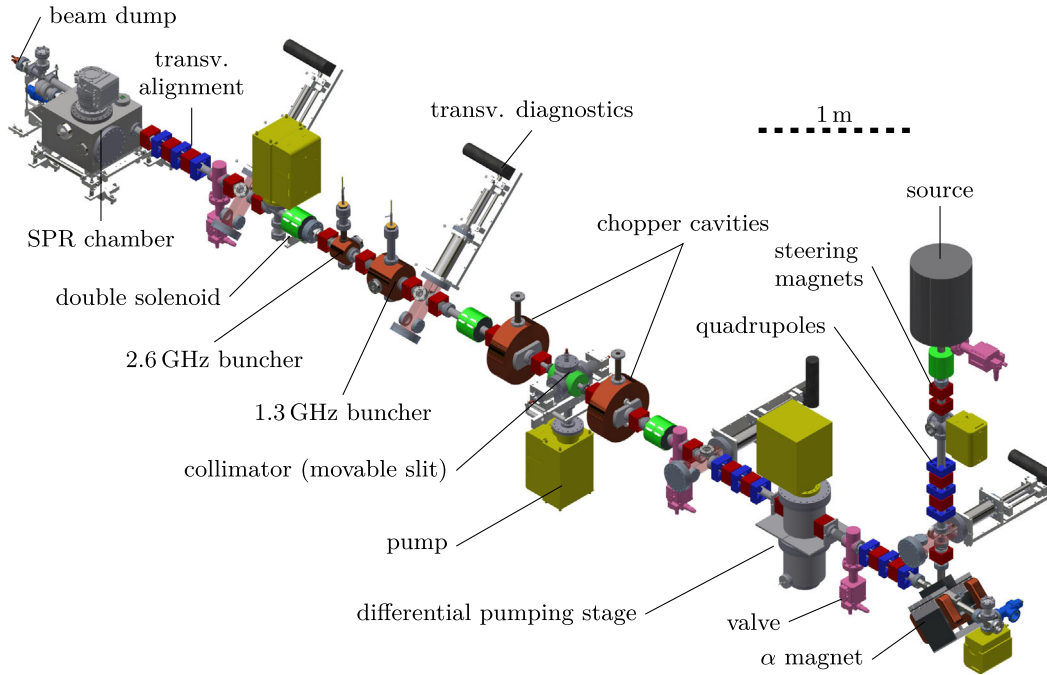
FIG. 3. Test apparatus for the injector of *MESA*. The DC electron beam from the source is chopped by two circularly deflecting rf cavities and an adjustable slit which cuts out a certain range of rf phases of the beam. Longitudinal compression is achieved with a system of two buncher cavities. Bunch length measurements are done in the SPR chamber. A quadrupole triplet including correction dipoles in front of the chamber provides transverse alignment of the beam.

10 pC. Since the coherent fraction scales with the square of the bunch charge, the coherent/incoherent ratio increases with bunch charge. Due to cw operation, the average power level is sufficiently large to be detected with our detector (> 2 pW) even for the lowest charge. To obtain information on the bunch shape, a spectrally resolved measurement is needed. To keep the apparatus simple, the SPR observation angle is fixed and gratings with varying periods are introduced to obtain spectral information on the coherent part. Table I summarizes the parameters of this experiment.

IV. BUNCHER SYSTEM

As the beam enters the buncher system at a nonrelativistic velocity of βc with $\beta = 0.548$, the longitudinal compression of the bunches is done using a phase-dependent velocity modulation $\Delta\beta$. For long drift spaces between the buncher cavities and the focal point ($L_f \gg \beta\lambda_{RF}$), the needed modulation $\Delta\beta$ is linear with respect to the entrance phase of the reference particle in the first buncher cavity ϕ_1.

$$\Delta\beta \approx \frac{\beta^2}{2\pi L_f} \cdot \phi_1 \qquad (5)$$

Such a linear velocity modulation can be achieved using a first- and second-harmonic buncher cavity. The system of two buncher cavities described in [9] was adapted to the fundamental rf frequency of 1.3 GHz of *MESA* (see [11]). The setup is shown in Fig. 4. With this arrangement, four free parameters have to be adjusted in order to obtain the best bunching result: the power in each cavity P_1 and P_2 and the corresponding phases ϕ_1 and ϕ_2 relative to the phase of the chopper cavities.

TABLE I. Parameters of the experiment.

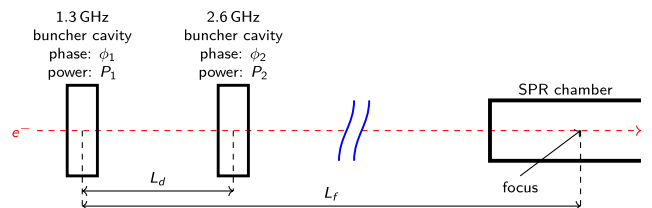|	
Bunch repetition rate	1.3 GHz
Beam energy	100 keV
β	0.548
Bunch charge	0.1 pC to 2.3 pC
Power SPR	2 pW to 50 nW
Wavelength SPR	≈ 1 mm

FIG. 4. Principle of longitudinal bunch compression using two cavities.

V. SPR SETUP

The SPR apparatus is installed downstream of the *MELBA* (see Fig. 3). Here, several different gratings can be placed next to the beam, and the detector is at a fixed position in order to keep the system simple (Fig. 5). This allows to get frequency-domain information about the bunch without the need to install potentially lossy and mechanically complicated angle-scanning THz optics. The SPR radiation leaves the vacuum system through a z-cut quartz window. The power of the signal is measured for each individual grating. If the grating period D is in the
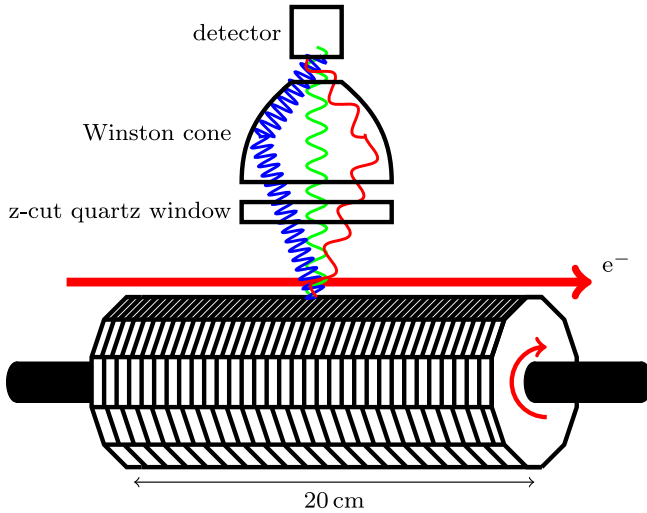

FIG. 5. Setup of the experiment. Multiple gratings can be placed next to the electron beam. The central observation angle is $\eta = \zeta = 0°$ with an angular spread of $\pm 2.1°$. The generated THz radiation with a power of some pW to 30 nW is observed with a bolometer cooled down to 4.2 K.
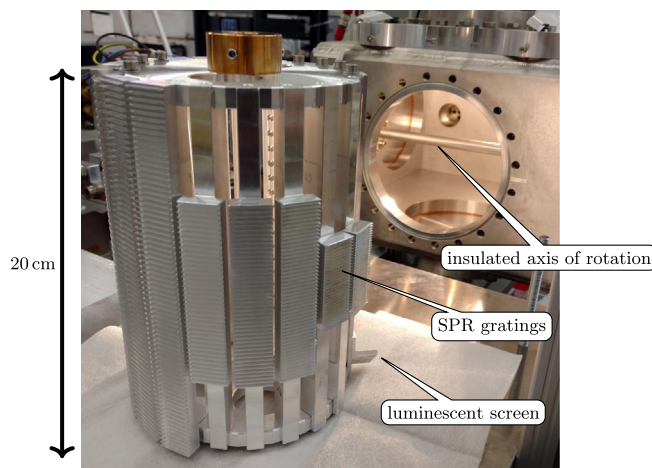

FIG. 6. Drum on which up to 20 gratings can be mounted (0.75 mm $< D < 6$ mm). Transverse diagnostic tools (screens, holes, and wires) are contained as well. When installed in the SPR chamber, the drum is mounted on an insulated, rotatable axis.
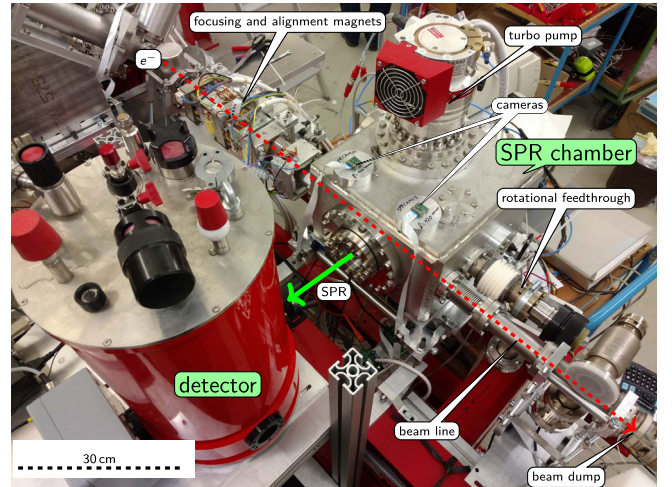

FIG. 7. Setup to detect SPR. The electron beam passes several magnets and is guided through the SPR chamber, in which the drum shown in Fig. 6 is mounted. The detector is placed directly in front of the vacuum window.

order of the bunch length, coherent enhancement of the SPR will increase the signal by a factor approaching N_e. The minimum period D below which the coherent signal disappears is closely related to the bunch length, see Fig. 2.

Figure 6 shows a picture of the drum with different gratings mounted. The insulated axis makes it possible to measure the current of the small part of the electron beam which hits the grating. This simplifies the transverse alignment of the beam. Figure 7 shows the finished setup. The detector is a thermally sensitive resistance cooled down to 4.2 K, which makes it possible to detect THz radiation with a power of 2 pW at an integration time of 30 s and a signal-to-noise ratio of one. The red cryostat which cools the resistance is moved as close as possible to the vacuum window in order to reduce losses of THz radiation in air.

VI. MEASUREMENTS

A. Adjusting the system of buncher cavities

In order to obtain short electron bunches at the location of the SPR grating, the four parameters of the buncher system (P_1, P_2, ϕ_1 and ϕ_2) have to be adjusted. This is achieved using the grating with the largest period ($D = 6$ mm). In the first measurement (Fig. 8), only the first-harmonic buncher cavity is turned on in order to reduce the number of free parameters to one phase ϕ_1 and one rf power P_1. A maximum of the emitted SPR can be observed at a phase of $\phi_1 \approx 270°$. The value for $P_1 = 15$ W is estimated from electromagnetic particle tracking simulations and a known shunt impedance of the cavity. In order to check if the signal results from coherent interaction, the bunch charge Q_b is increased at $\phi_1 = 270°$ and the rise of the signal is measured. Looking at Eq. (2), the SPR signal
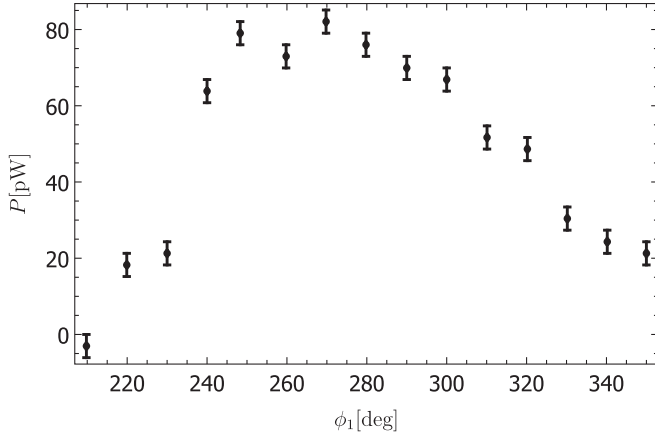
FIG. 8.   SPR power P to the phase of the first-harmonic buncher cavity ϕ_1 at a fixed value of $P_1 = 15$ W. The second buncher cavity is turned off.

should rise with the square of the number of electrons per bunch N_e.

$$\frac{dP}{d\Omega} \propto N_e^2 \cdot S_{coh} \tag{6}$$

Here, the beam current $I = Q_b f = N_e f e$ is expressed in terms of electrons per bunch with the repetition rate of *MESA* of $f = 1.3$ GHz and the elementary charge e. Figure 9 shows the measured behavior of the detected SPR power P for different bunch charges Q_b or the number of electrons per bunch N_e, respectively. Here, Q_b is changed by variation of the power of the laser hitting the photocathode. A rise of the detected signal with respect to the square of the bunch charge can be observed. This means that the bunch length σ_x is smaller than roughly
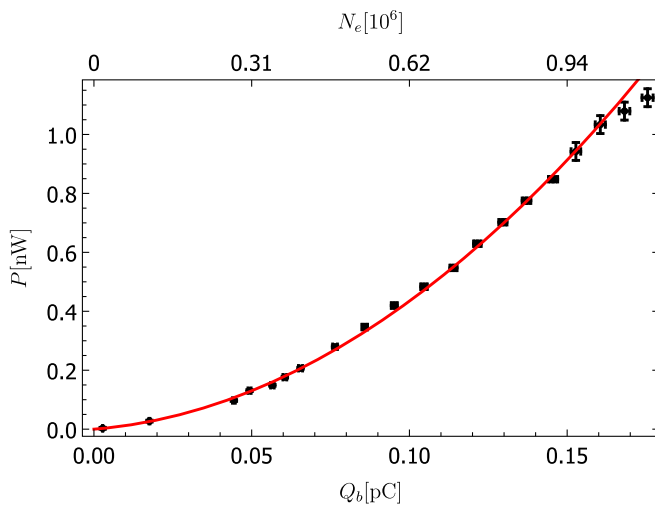

FIG. 9.   SPR power P for different bunch charges Q_b. A rise of P as the square of Q_b can be observed, proving that a coherent effect is detected.
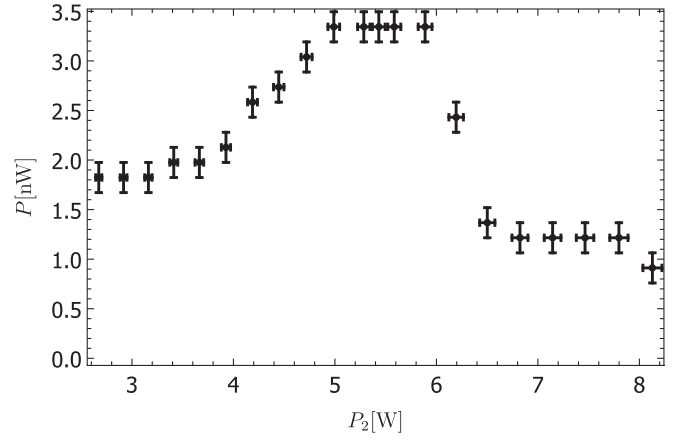

FIG. 10.   SPR power P vs. power of the second-harmonic buncher cavity P_2 at the smallest grating period $D = 0.75$ mm.

$D/2 = 3$ mm. Other, potentially coherent, background radiation can be excluded (see Sec. VI D).

The method described above is repeated for smaller grating periods D until the best set of parameters (P_1, P_2, ϕ_1 and ϕ_2) is found at the smallest $D = 0.75$ mm. Figure 10 shows an example of the measured SPR signal P for different powers of the second-harmonic buncher cavity P_2. A maximum of the emitted SPR can be observed at $P_2 \approx 5.5$ W. In analogy to Fig. 9, a variation of the bunch charge leads to a quadratic rise of the signal. Therefore, the bunch length must be smaller than $\sigma_x \lesssim D/2 = 375$ μm, and the optimum parameters of the buncher system are $P_1 = 15.2$ W and $P_2 = 5.4$ W. The phases ϕ_1 and ϕ_2 do not contain relevant information because they depend on experiment-specific parameters such as cable length. Electromagnetic simulations have shown that it is possible to operate the preaccelerator for *MESA* (*MAMBO* [12]) with an energy width of $\Delta E_{RMS,design} = 1.022$ keV and a bunch length of $\sigma_{x,design} = 1.7$ mm at the entrance of the first acceleration section [13]. The measured bunch length of $\sigma_x \gtrsim 375$ μm and the produced energy width with the set parameters P_1 und P_2 of $\Delta E_{RMS} \approx 1$ keV therefore exceeds the requirements.

B. Further bunch length investigation

Until now, only an upper limit for the bunch length has been determined. In order to obtain a more precise value of σ_x, a comparison of the calculated SPR power with the measured one can be done. For the calculation of the emitted SPR power in particular, all beam parameters entering Eq. (2) and Eq. (3) have to be known. The transverse beam profile is measured with luminescent screens, and the beam current can be determined using a Faraday cup (here beam dump). Additionally the reflection coefficient $|R_n|^2$ has to be calculated (see Sec. VI C). Figure 11 shows a measurement in which the distance between beam and grating z_0 (see Fig. 1) is varied. With this method, a fixed value for the bunch length of $\sigma_x =$
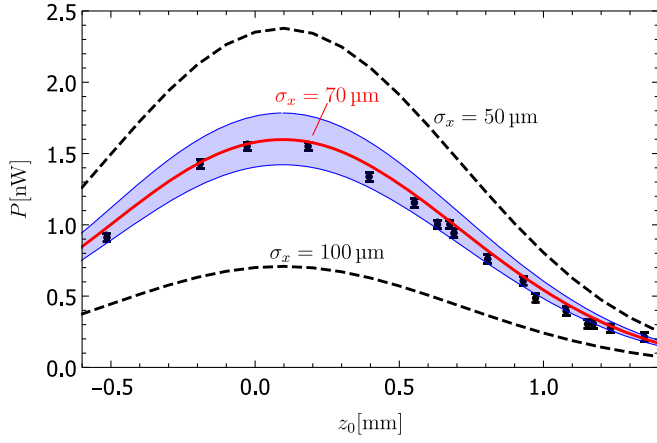
FIG. 11.   SPR power P vs. distance between beam and grating z_0. Red curve: Calculated behavior [Eq. (2)] with corresponding error (blue) for $Q_b = (270 \pm 10)$ fC, $\sigma_z = \sigma_y = (866 \pm 15)$ μm and a bunch length of $\sigma_x = (70 \pm 5)$ μm. The dotted lines indicate the calculated behavior for $\sigma_x = 50$ μm and $\sigma_x = 100$ μm.

(70 ± 5) μm can be determined. In this calculation, an error of the reflection coefficient of $\Delta|R_n|^2 = \pm 20\%$ is assumed (see Sec. VI C).

C. Reflection coefficient

Referring to Eq. (2), the emitted SPR is proportional to the reflection coefficient $|R_n|^2 = |R_n|^2(n, \beta, \eta, \zeta, a/D, h/D)$, where a and d describe the geometry of the respective grating (see Fig. 12). It is possible to calculate $|R_n|^2$ for rectangular gratings numerically with the approach of van den Berg. In this experiment five different geometries are chosen. Note that gratings with different periods D can have the same fractions a/D, h/D and thus the same reflection coefficient. Table II shows the values of the calculated reflection coefficients for the observation angle of $\eta = \zeta = 0°$. In order to get a strong signal, a high value of the reflection coefficient is favorable.

The errors of the coefficients are estimated in a dedicated experiment: Gratings with the same period D but with different geometries are successively placed next to the electron beam without changing any beam parameters. The measured SPR powers are then compared and the deviation from its theoretical behavior is investigated.

One has to note that multiple radiation orders n are always observed at the same time by the detector. A more precise analysis of the reflection coefficient at a specific order of radiation n was done by using a multiwire grid band-pass filter which is placed between the grating and the
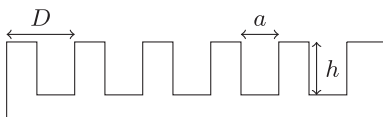

FIG. 12.   Geometry of the gratings.

TABLE II.   Reflection coefficients for $\eta = \zeta = 0°$ and $\beta = 0.548$ in the first three radiation orders n and different geometries.

a/D	h/D	$|R_1|^2$	$|R_2|^2$	$|R_3|^2$
0.80	0.92	0.4×10^{-3}	14×10^{-3}	0.1×10^{-3}
0.27	0.57	0.35	47×10^{-3}	0.86×10^{-3}
0.33	1.04	83×10^{-3}	95×10^{-3}	8.8×10^{-3}
0.35	1.66	80×10^{-3}	1.9×10^{-3}	2.1×10^{-3}
0.26	1.80	2.1×10^{-3}	11×10^{-3}	4.4×10^{-3}

detector. This filter is chosen in such a way that only one order of radiation n of the SPR is transmitted.

With these investigations, an error for the reflection could be estimated: In sum over all observable radiation orders n, the reflection coefficients are assumed to have an error of roughly 20%. As a preliminary result, a suppression of high values for the reflection coefficients could be observed. Especially the high value of 0.35 in Table II could be disproved. At this point, further investigations with more band-pass filters and an experimental determination of the coefficients with known bunch length are needed to discuss this problem in an adequate manner.

D. SPR as a minimally invasive measurement tool

As seen in Fig. 11, the SPR signal P decreases fast with growing distance between beam and grating z_0. Nevertheless, a signal can be observed at high values of z_0. In the following measurements, the transverse shape of the beam is not changed. In Fig. 13, the bunch charge Q_b is varied for five different distances between beam and grating. The SPR signal rises with the square of Q_b, as observed in Fig. 9. Therefore, the signal must be coherent, and bunch length measurements can be done while losing less than 0.6% of the beam in the case of $z_0/\sigma_z = 2.54$. The dashed curves describe a quadratic fit of the data:
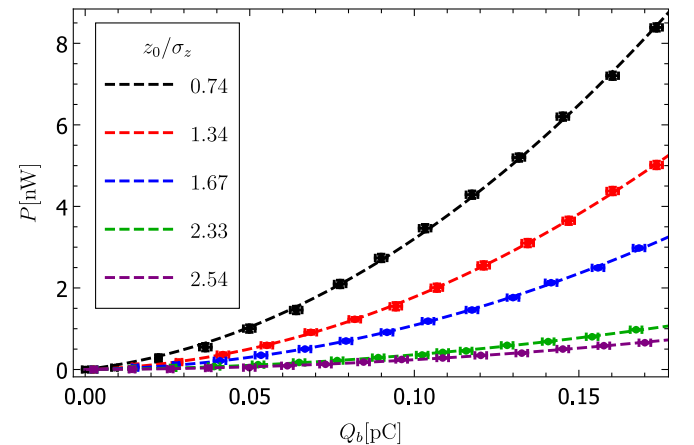

FIG. 13.   SPR power P to bunch charge Q_b for different distances between beam and grating z_0. The transverse size of the beam $\sigma_z \approx 100$ μm is not changed.

TABLE III. Fit parameters of the dashed curves in Fig. 13.

z_0/σ_z	a [nW/pC]	b [nW/pC^2]	a/b [10^{-3} pC]
0.74 ± 0.04	9.81 ± 1.41	223 ± 11	44.0 ± 6.7
1.34 ± 0.02	2.38 ± 0.93	154 ± 7	15.5 ± 6.1
1.67 ± 0.02	1.08 ± 0.46	97.4 ± 3.9	11.1 ± 4.8
2.33 ± 0.07	0.46 ± 0.15	31.4 ± 1.3	14.6 ± 4.9
2.54 ± 0.06	0.22 ± 0.12	21.8 ± 0.9	10.1 ± 5.7

$$P = a \cdot Q_{\mathrm{b}} + b \cdot Q_{\mathrm{b}}^2. \qquad (7)$$

The parameters a and b are listed in Tab. III. The fraction a/b decreases with growing distance z_0. This means that linear effects are less significant at larger distances between beam and grating. Fig. 14 shows the linear part of the signal a for the five set distances z_0/σ_z. The linear part of the signal a can be explained by calculating how many electrons are getting lost on the grating. The transverse particle distribution [$f_z(z)$ in Eq. (3)] is known. Integrating this distribution up to the surface of the grating ($z_0 = 0$) yields the red curve in Fig. 14 with the corresponding error band in blue. This means that particles which hit the grating produce a linear background signal, and the coherent part of the signal is only caused by electrons which do not hit the grating. This property of the observed radiation can only be described by the underlying mechanism of SPR.

E. Space charge effects

Coulomb interactions between the electrons lead to a blow-up of the particle distribution at higher bunch charges. In Fig. 15, the bunch charge is increased up to $Q_{\mathrm{b}} \approx 0.75$ pC and the bunch length σ_x is determined by comparing the calculated and measured SPR power. The black curve shows the behavior for the fixed values for the buncher system (P_1, P_2, ϕ_1 and ϕ_2) described in Sec. VI A. In this measurement, space charge mostly affects the
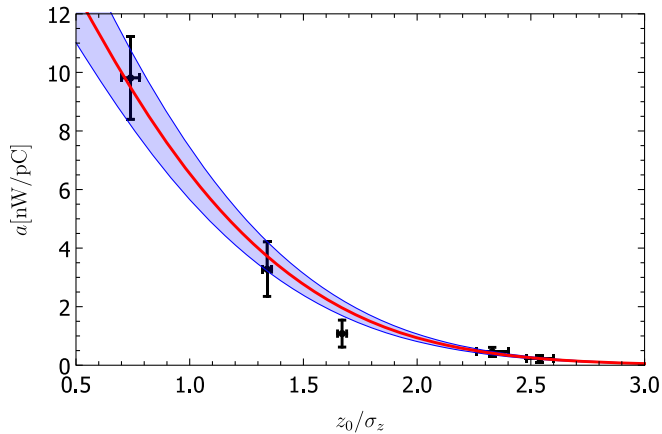

FIG. 14. Linear part of the SPR signal a shown in Fig. 13 for the five different applied distances (values from Table III).
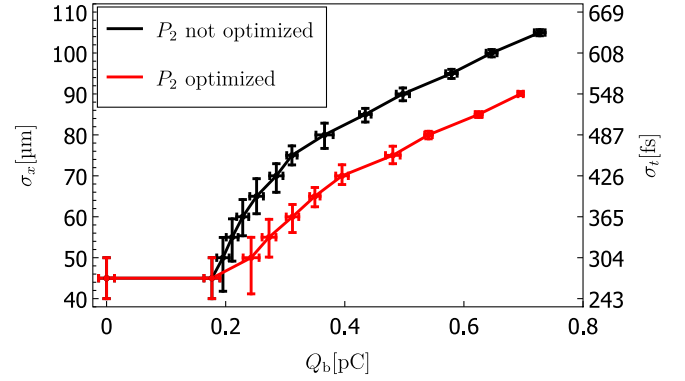

FIG. 15. Bunch length σ_x to bunch charge Q_{b}. The power of the second-harmonic buncher cavity P_2 is optimized for different bunch charges.

longitudinal particle distribution. Simulations have shown that the relative increase of the transverse beam size (here $\sigma_y = \sigma_z \approx 870$ μm) due to space charge is about 15%. This effect can be neglected here because the change in the emitted SPR power P at a variation of $\Delta\sigma_z = \pm15\%$ is low. In Fig. 15, the impact of space charge on the longitudinal particle distribution can be observed starting at bunch charges of $Q_{\mathrm{b}} \approx 0.2$ pC. At smaller Q_{b}, no change in σ_x can be observed within the resolution of our detection system. Thus, the nonlinear effect of the space charge has to be considered only for $Q_{\mathrm{b}} > 0.2$ pC at a transverse beam size of $\sigma_z \approx 870$ μm. At this point, the electron density becomes high enough for the Debye-length [14] to be small compared to the spacial dimensions of the bunch.

Considering nonlinear effects, the best velocity modulation is not necessarily linear as assumed in Eq. (5). So the increase in σ_x can be compensated for to a certain point by re-adjusting the four parameters of the buncher system in order to obtain a better, yet unknown, velocity modulation. For example, a variation of the power of the second-harmonic buncher cavity P_2 is adjusted for bunch charges greater than 0.2 pC (red curve in Fig. 15). Here, a shortening of the bunch length σ_x by approximately 10% can be achieved by increasing the power P_2 from 5.4 W at low bunch charges to 8.2 W at $Q_{\mathrm{b}} = 0.75$ pC.

VII. LIMITATION OF BUNCH LENGTH DETERMINATION

The bunch length measuring limit with the method described is defined by the grating period D. If $\sigma_x \ll D$, the coherent enhancement factor S_{coh} (see Fig. 2) saturates and changes in the bunch length cannot be resolved by the detection system. Figure 16 shows the calculated SPR power for short bunch lengths at the smallest available grating of $D = 0.75$ mm. So the available detection system provides a bunch length measuring limit of roughly 10 μm at a grating with $D = 0.75$ mm.
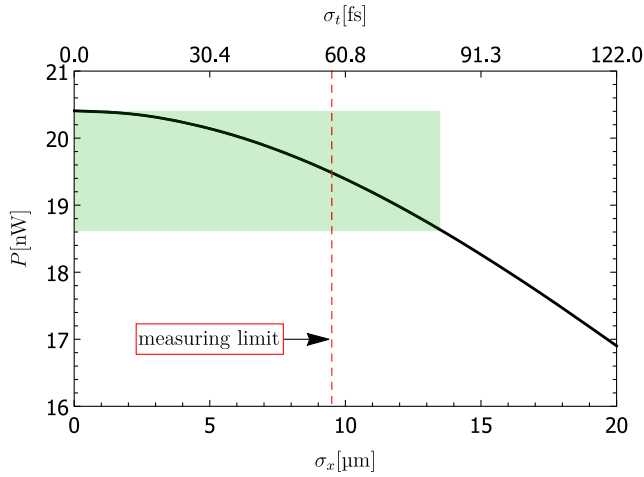
FIG. 16. Calculated SPR power for short bunch lengths at the smallest available grating period $D = 0.75$ mm. At a bunch length of $\sigma_x \lesssim 10$ μm, changes in σ_x cannot be resolved by the detection system. The green box indicates the measuring accuracy of the detection system of $\pm 4.4\%$.

VIII. CONCLUSION

It was shown that coherent Smith-Purcell radiation can be used to measure bunch lengths at a test apparatus for the *MESA* accelerator. It is an minimally invasive method whereby less than 0.6% of the beam is lost. This makes it possible to do live measurements even at high beam currents. The observation of a coherent effect at a grating with known constant D defines an upper limit of the bunch length. More precise results can be obtained by comparing the measured data with theory.

The achievable bunch length makes it possible to operate *MESA* with bunch charges of 0.75 pC, which essentially fulfills the specifications for the operation of *MESA* in its first stage. In addition, there are other conceivable applications of the measurement method: Ultrafast processes on surfaces can be observed with time-resolved electron microscopes. Therefore, short electron pulses of about 100 fs are needed with typical energies of 1 keV to 100 keV, which is in the same order of magnitude as the experiment carried out.

For future measurements, it would be favorable to use calibrated SPR gratings. To obtain these, an alternative invasive bunch length measuring method using a deflecting cavity and a luminescent screen can be used. The SPR power is then measured with the knowledge of all beam parameters. By using band-pass filters, each radiation order n can be observed separately. With this method, the reflection coefficient $|R_n|^2$ can be determined with better accuracy and for all orders n. Such a calibrated grating could then be used to obtain even more precise results.

Depending on the bunch charge, other detector systems without the need to be cooled to 4 K can be used if the signal is strong enough. Then, a more compact design of the whole apparatus can be applied even at space-limited machines.

[1] P. M. van den Berg, J. Opt. Soc. Am. **63**, 1588 (1973).
[2] P. M. van den Berg and T. H. Tan, J. Opt. Soc. Am. **64**, 325 (1974).
[3] S. J. Smith and E. M. Purcell, Phys. Rev. **92**, 1069 (1953).
[4] B. Hua and D. Zhi-Min, Chin. Phys. C **32**, 916 (2008).
[5] C. Matejcek, Strahldynamik der Niederenergie-Strahlführung von MESA unter Berücksichtigung von Raumladung und Multipol-Beiträgen höherer Ordnung, Ph.D. thesis, Johannes Gutenberg-Universität Mainz, 2020.
[6] S. Friederich, Entwicklung einer hochbrillanten Photoemissionsquelle für spinpolarisierte Strahlen, Ph.D. thesis, Johannes Gutenberg-Universität Mainz, 2019.
[7] P. Heil, Kohärente Smith-Purcell-Strahlung zur minimal invasiven Bunchlängenmessung im Subpikosekundenbereich, Ph.D. thesis, Johannes Gutenberg-Universität Mainz, 2020.
[8] S. Friederich, K. Aulenbacher, and C. Matejcek, in *Proceedings of the 10th Int. Particle Accelerator Conf. IPAC2019, Melbourne, Australia* (JACoW, Geneva, 2019).
[9] V. I. Shvedunov *et al.*, Conf. Proc. C **960610**, 1556 (1996).
[10] G. Doucas, M. F. Kimmitt, A. Doria, G. P. Gallerano, E. Giovenale, G. Messina, H. L. Andrews, and J. H. Brownell, Phys. Rev. Accel. Beams **5**, 072802 (2002).
[11] P. Heil, Longitudinale Emittanzanpassung durch Geschwindigkeitsmodulation im Injektionssystem an MESA, Master's thesis, Johannes Gutenberg-Universität Mainz, 2015.
[12] F. Hug and R. Heine, J. Phys. Conf. Ser. **874**, 012012 (2017).
[13] R. Heine, Phys. Rev. Accel. Beams **24**, 011602 (2021).
[14] T. P. Wangler, *RF Linear Accelerators* (Wiley-VCH GmbH, New York, 2008).